Applied Catalysis B: Environmental 338 (2023) 123019

Contents lists available at ScienceDirect

Applied Catalysis B: Environmental

journal homepage: www.elsevier.com/locate/apcatb

Electrochemical NH_3 production: *In-situ* evaluation of the activity and durability of nitrogen-reduction catalysis using scanning electrochemical microscopy (SECM)

Jimin Kong [a,b], Hansung Kim [b,*], Hyun S. Park [a,c,**]

[a] Hydrogen·Fuel Cell Research Center, Korea Institute of Science and Technology (KIST), Seoul 02792, Republic of Korea
[b] Department of Chemical and Biomolecular Engineering, Yonsei University, Seoul 03722, Republic of Korea
[c] Division of Energy & Environment Technology, KIST School, University of Science and Technology (UST), Seoul 02792, Republic of Korea

ARTICLE INFO

Keywords:
Ammonia synthesis
Electrocatalyst
Nitrogen reduction
Scanning electrochemical microscopy
Ammonia oxidation

ABSTRACT

Developing efficient electrochemical processes for ammonia (NH_3) production is a significant challenge that needs to be met to realize a carbon-neutral chemical industry. Recently, electrocatalytic nitrogen-reduction has been actively investigated under ambient conditions. However, the evaluation of electrodes for NH_3 production using *ex-situ* NH_3 detection methods only provide time- and space-averaged catalytic information. When investigating the transient activity of electrodes with spatiotemporal information, the real-time detection of NH_3 near the electrode with high analytical resolution is essential. In this study, *in-situ* detection of electrochemically generated NH_3 was first demonstrated using scanning electrochemical microscopy. A low NH_3 flux of 6.6 nmol cm^{-2} s^{-1} generated from an Fe-CuS/C electrode was detected using NH_3 oxidation current detected at a polycrystalline Pt ultramicroelectrode. This observation provides invaluable information on catalysis, including transient activity and durability. The advantages and limitations of the proposed *in-situ* NH_3 detection method are demonstrated in an evaluation of nitrogen-reduction electrolysis.

1. Introduction

With an annual production of 146 million tons, ammonia (NH_3) is the second-most commonly synthesized chemical worldwide [1]. It is intensively used as feedstock for nitrogen-containing chemicals, textiles, fertilizer, and medicines [2]. It has also been proposed as a zero-carbon hydrogen carrier for large-scale and long-term storage because it is easily liquefied under mild conditions (0.8 MPa and 25 °C) and has a high hydrogen content of 17.6 wt% [3]. Since 1913, industrial NH_3 has been mainly produced using the Haber–Bosch process [4], which is an energy-intensive thermochemical method conducted at high temperatures of 300–550 °C and a high pressure of 250 bar [5]. This process on its own accounts for approximately 2% of the world's energy consumption and produces 2.9 tons of CO_2 ton_{NH3}^{-1}, making up approximately 2% of the total global greenhouse gas emissions [6]. Thus, novel NH_3 production methods that are environmentally and economically sustainable and overcome the problems created by the Haber–Bosch process are urgently required.

Among many different methods, direct nitrogen-reduction electrocatalysis has been suggested as a promising carbon-free route for sustainable and scalable NH_3 production [7]. Given that the hydrogen required for the reaction is supplied via water electrolysis and the entire process is powered by using renewable energy sources, an electrochemical reactor emits only pure oxygen as the byproduct in NH_3 production. However, the hydrogenation of nitrogen molecules is known to exhibit particularly sluggish kinetics at ambient temperatures. As a result, the development of effective catalysts for the electrochemical nitrogen-reduction reaction (e-NRR) is essential for practical NH_3 production.

The e-NRR activity of developed catalysts is often estimated by measuring the amount of NH_3 dissolved in the electrolyte and the acid trap solutions in electrochemical cells [8]. Various analytical methods have been used to quantify the amount of NH_3, including indirect spectrophotometric detection using Nessler reagent, indophenol, or salicylic acid reactions and direct detection via liquid chromatography (LC) [9], ion chromatography (IC), [10] and nuclear magnetic resonance

* Corresponding author.
** Corresponding author at: Hydrogen·Fuel Cell Research Center, Korea Institute of Science and Technology (KIST), Seoul 02792, Republic of Korea.
E-mail addresses: elchem@yonsei.ac.kr (H. Kim), hspark@kist.re.kr (H.S. Park).

https://doi.org/10.1016/j.apcatb.2023.123019
Received 7 March 2023; Received in revised form 7 June 2023; Accepted 18 June 2023
Available online 20 June 2023

(NMR) [11]. The *ex-situ* detection of NH_3 or its derivatives after e-NRR experiments is useful with low detection limits and a high resolution. For example, 0.02 ppm NH_3 in a liquid electrolyte can be detected using spectrophotometric techniques [12]. The NH_3 concentration required for measurements is thus achieved via the chronopotentiometric operation of an e-NRR electrode, for example, with an electrode at 0.019 mA in 100 mL of electrolyte requiring 30 min to reach the minimum concentration for detection. However, these electrodes are often unstable when performing sustained experiments, so the subsequent e-NRR activity and stability measurements may not be accurate. It is also difficult to monitor transient behavior or the durability of an e-NRR electrode without the *in-situ* detection of NH_3 near the surface of the electrode. Moreover, any contamination by atmospheric NH_3 impurities in the *ex-situ* detection can hinder accurate measurements of e-NRR activity of catalysts.

To overcome the problems associated with *ex-situ* NH_3 detection methods, approaches for the *in-situ* detection of NH_3 produced by e-NRR electrodes have been developed [13,14]. For example, Krempl et al. [25] reported the *operando* detection of electrochemically synthesized NH_3 from nitrogen-reduction via Li-mediated methods using an electron ionization mass spectrometer (EI-MS). They reported that NH_3 generated in aqueous and non-aqueous electrolytes was transported out of the reactor and could be quantitatively detected up to a level of 1 pmol s^{-1} using selective ionization at 22 eV with a highly sensitive micro-chip-based electrochemical mass spectrometer setup. Ripepi et al. [20] reported an *operando* NH_3 detection method using gas chromatography-mass spectrometry (GC-MS). Although their analytical method could directly quantify gaseous $^{14}NH_3$ and $^{15}NH_3$ in the reactor head-space, the MS analysis still needs to discharge the produced NH_3 to the outside of the electrochemical cell, thus requiring a delay time for the transport.

Neither the *in-situ* detection of NH_3 near the e-NRR electrode with millisecond resolution during NH_3 production nor the use of scanning electrochemical microscopy (SECM) in e-NRR research has previously been reported. SECM is an electrochemical scanning probe technique developed by Allen J. Bard in 1989 [15]. In this approach, an ultramicroelectrode (UME) with a diameter of 100 μm to a few nm is attached to an XYZ positioner to investigate or modify a substrate positioned directly below the probe electrode. As an analytical tool, it measures the electrochemical reactions at the UME originating from local redox chemicals produced from and/or consumed on the substrate, so the physical, chemical, and electrochemical properties of the substrate are estimated based on space coordinate information [16]. By using SECM in the development of electrocatalysts, the electrocatalytic performance of electrodes can be measured within a few tens of milliseconds by quantifying the amounts of chemicals generated in the vicinity of the catalyst [17]. SECM can also provide information on the reaction dynamics, topographical features, and the distribution of reactive sites in a catalytic system through the spatial activity mapping of the substrate [18].

Monitoring localized catalytic electrochemical reactions *in-situ* can lead to the development of effective catalysts and enable accurate research. With the characteristics of the technology that can effectively provide various pieces of information, many investigations of electrochemical reactions such as oxygen reduction [19], water electrolysis [20], methanol oxidation [21], and carbon dioxide reduction [17] have been reported. As an electroanalytical tool, SECM is an advanced *in-situ* electroanalytical technique that can be used to investigate electrodes by providing spatiotemporal information such as the spatial uniformity of reactions over the catalyst surface and long-term changes in catalytic activity with a low detection limit. However, *in-situ* detection using SECM technique has not yet been reported for the e-NRR process, to the best of our knowledge.

In the present study, the substrate generation (SG)–tip collection (TC) mode of SECM was employed to evaluate an Fe-CuS/C catalyst for the e-NRR. To realize the real-time detection of NH_3 produced at an e-NRR electrode, a polycrystalline Pt UME with a diameter of 25 μm was fabricated to enhance the NH_3 oxidation reaction (AOR) current as a probe signal. The developed Pt UME was then equipped with an SECM system for the concentration mapping of locally distributed NH_3 in an aqueous solution. Finally, SECM was employed to evaluate the Fe-CuS/C, e-NRR catalyst, and the time-dependent activity and stability of the catalyst were then compared to the results obtained from an *ex-situ* analysis. Thus, in the proposed system, a metal sulfide catalyst reduced the nitrogen dissolved in basic aqueous solutions to generate NH_3 at the e-NRR electrode, and the Pt UME equipped with the SECM system detected the NH_3 dissolved near the electrode. The activity of the catalyst was determined in real-time using SECM analysis during electrochemical NH_3 synthesis, and information on the transient degradation process of the catalyst was also obtained. The electrochemical probe detection of NH_3 using SECM for e-NRR electrodes opens a new route for the development of effective e-NRR catalysts by rapidly providing valuable information on nitrogen-reduction catalysis that cannot be obtained using currently available analytical techniques.

2. Experimental

2.1. Chemicals

Chloroplatinic acid solution (8 wt% in H_2O), iron(III) chloride ($FeCl_3$, 97%), ammonium hydroxide solution (28% NH_3 in H_2O, ≥99.99%), sodium sulfide, copper(II) chloride ($CuCl_2$, 99%), thiourea (≥99.0%), formic acid (ACS reagent, ≥96%), potassium ferricyanide(III) ($K_3Fe(CN)_6$, 99%), potassium hexacyanoferrate(II) trihydrate ($K_4Fe(CN)_6$•3 H_2O, ≥ 99.95%), aqueous polytetrafluoroethylene (PTFE) solution (60 wt% dispersion in H_2O) and potassium hydroxide (KOH, ≥ 85%) were all purchased from Sigma-Aldrich. Ethyl alcohol (95%) was obtained from Samchun Chemicals. All of the chemical reagents were used without further purification. Carbon paper (TGP-H-120) was obtained from Toray. Highly pure Ar and nitrogen (99.999%) were purchased from Shinyang Oxygen Industry Co., Ltd.

Catalyst Synthesis An Fe-CuS/C catalyst (0.5 at%) was used for the e-NRR. First, 12 mM $CuCl_2$, 21 mM thiourea, 8.0 mM $FeCl_3$, and carbon (Ketjenblack) were dissolved in ethanol at room temperature and stirred for 2 h. The powder was then separated from the suspension and washed using vacuum filtration, after which the filter cake was dried in a vacuum oven set at room temperature. After grinding the filter cake, it was heat-treated at 200 °C for 2 h under a flow of Ar. The temperature was increased at a ramping rate of 5 °C min^{-1} from room temperature to 200 °C.

Electrode Fabrication NRR electrodes (0.33 cm^2) were prepared by spraying a catalyst ink onto carbon paper. The catalyst ink was produced by mixing catalyst powder, aqueous PTFE solution, isopropyl alcohol, and deionized (DI) water (18 MΩ). Following this, 1 mg cm^{-2} of the active catalyst was loaded onto the electrode. The catalyst-coated electrode was then calcined for 5 min at 350 ℃ in an Ar atmosphere. The ramping rate was 1 ℃ min^{-1} from room temperature to 350 ℃.

2.2. Probe preparation

The probe tip used for SECM was a 25 μm diameter Pt UME (Bio-Logic, U-P5/25) with an RG ratio of approximately 10. The RG is the ratio between the outer diameters of the electrode including the glass sheath to the size of the active Pt electrode. Optical microscope images of the pristine UME are presented in Fig. 1(a). Polycrystalline Pt was layered on top of the Pt UME using chemical and electrochemical processes. For the chemical deposition of polycrystalline Pt, 500 μL of formic acid was added to 12.5 mL of DI water at 18 °C, after which 100 μL of H_2PtCl_6 solution was added. Finally, the pristine Pt UME was placed for 1 h in the well-mixed solution at a temperature of 40 °C. The deposition of Pt occurred via the following reaction:

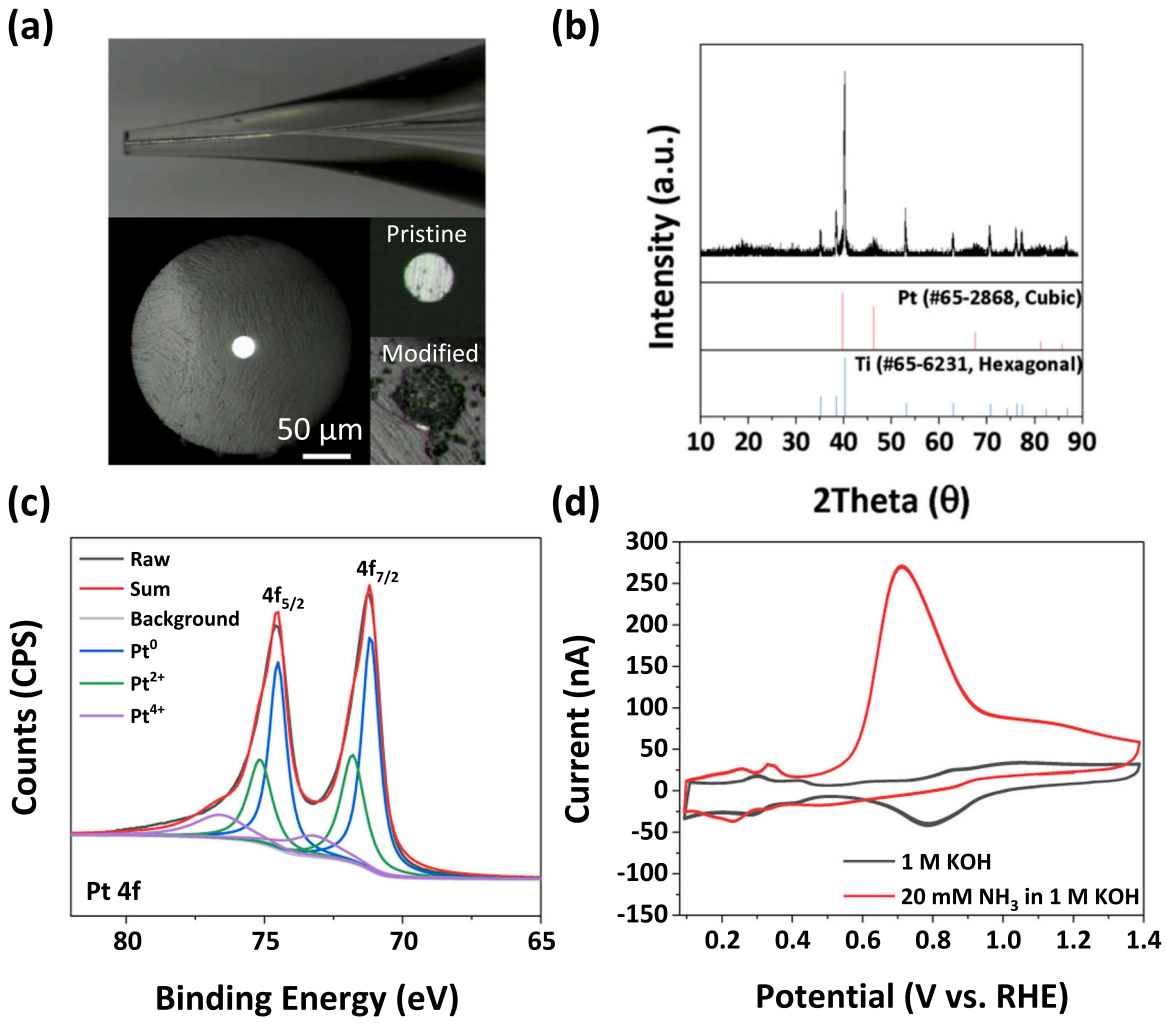

Fig. 1. (a) Optical microscope images of the pristine and modified Pt UMEs. (b) An XRD pattern and (c) XPS Pt 4 f spectra of the Pt species deposited on a Ti PTL. (d) Cyclic voltammograms at the modified Pt UME in 1 M KOH aqueous solution with and without NH_3 at a scan rate of 20 mV s^{-1}.

$$H_2PtCl_6 + 2HCOOH \rightarrow Pt + 6HCl + 2CO_2\uparrow \quad (1)$$

After the reaction had completed, the modified Pt UME was washed using copious amounts of ethanol and DI water. All of the electrochemical analyses were conducted using the modified Pt UME unless otherwise specified.

2.3. Tip positioning

Before conducting SG-TC mode of SECM, the Pt UME was aligned by measuring the approach curves in an aqueous solution of 5 mM $K_3Fe(CN)_6$, 5 mM $K_4Fe(CN)_6$, and 1 M potassium chloride (KCl). A controlled area of the active e-NRR electrode was exposed to the electrolyte while most of the electrode was covered by an insulating polymer film. A negative feedback curve of SECM was monitored over the polymer film by measuring the $[Fe(CN)_6]^{3-}/[Fe(CN)_6]^{4-}$ reduction current at the Pt UME at 0.41 V_{RHE} as the distance between the tip and the substrate was decreased. The tip-to-substrate distance (d) was fixed at 30 μm or at an i_{tip}/i_{bulk} ratio of 0.6. The value of d was estimated by fitting experimental approach curves to the calculated curve by using the following equation: [22].

$$I_T^{ins}(L) = i_T/i_{T,\infty} = 1/(A + B/L + C\exp(D/L)) + (EL)/(F + L)) \quad (2)$$

where $A = 0.4571825$, $B = 1.4604238$, $C = 0.4312735$, $D = -2.350667$, $E = -0.145437$, and $F = 5.5768952$ for RG = 10.

2.4. SG-TC mode of SECM

SECM was conducted using the e-NRR for SG and AOR for TC at the Fe-CuS/C catalyst and the Pt UME (SECM 470, BioLogic). Electrochemical measurements were taken using a three- and four-electrode configuration with the catalyst-loaded carbon paper and the Pt UME as the substrate and tip electrodes, respectively, a Pt wire as the counter electrode, and a saturated calomel electrode (SCE) in a saturated aqueous KCl solution as the reference electrode at room temperature. The experiment was conducted in a nitrogen-saturated 1 M KOH aqueous electrolyte under diffusion-controlled environments without convection. To detect NH_3 at the Pt UME (TC), cyclic voltammetry (CV) analysis of the probe was conducted to measure the AOR current at potentials ranging from 0.09 to 1.39 V_{RHE} at a scan rate of 20 mVs^{-1}. Electrochemical NH_3 generation was carried out at the Fe-CuS/C catalyst (SG) by applying −0.2 V_{RHE} to the substrate. To remove the background current including the reduction of surface oxides at Pt UME, the electrode was conditioned at an open-circuit potential for 20 s before each stage of SG-TC mode of SECM.

2.5. Bulk e-NRR electrolysis

e-NRR catalysis using the bulk Fe-CuS/C electrode was carried out in

an H-cell, with the Fe-CuS/C electrode and reference electrode in the same chamber and the counter electrode in another chamber. The two chambers were physically separated using an anion exchange membrane separator (FAA-3–75, Fumatech) treated in 1 M KOH for 24 h and washed with DI water before use. The experiment was conducted with a three-electrode configuration: carbon paper loaded with the catalyst (Fe-CuS/C) was used as the working electrode while a carbon rod and an SCE were used as the counter and reference electrodes, respectively. The bulk activity and durability of the Fe-CuS/C electrode were measured in a nitrogen-saturated 0.1 M KOH electrolyte. To investigate the e-NRR activity of the bulk Fe-CuS/C electrode, chronoamperometry (CA) was conducted for 30 min over a potential range of 0.0 to −0.6 V_{RHE}, with the generated NH_3 analyzed using the indophenol method (Fig. S1(a)). The electrolyte was swapped for a fresh solution before applying the potential to the electrode. The transient change in the e-NRR activity of the bulk electrode was estimated by measuring the increase in the NH_3 concentration of an aliquot taken from the aqueous 0.1 M KOH solution every 10 min, while the bulk Fe-CuS/C electrode in the nitrogen-saturated solution was constantly held at −0.2 V_{RHE} for 60 min

2.6. Ex-situ NH_3 quantification

The NH_3 concentration in the aqueous electrolyte solution was colorimetrically determined using the indophenol method [23]. Before detection, a phenol solution (0.64 M C_6H_5OH, 1.3 mM sodium nitroprusside ($C_5FeN_6Na_2O$), and 0.38 M sodium hydroxide (NaOH)) and a hypochlorite solution (55 mM NaOCl and 0.75 M NaOH) were prepared. Following this, 1 mL of the electrolyte from the cathodic reactor in the e-NRR experiments was added to a blank cuvette followed by 1 mL each of the phenol and hypochlorite solutions. After 1 h at room temperature, UV–vis spectroscopy was conducted by using a Cary UV–visible 100 spectrophotometer (Agilent) over a wavelength range of 350–875 nm. To quantify the concentration, the absorbance measured at a wavelength of 632 nm was plotted against the concentration of NH_3. The calibration curves obtained from the indophenol method are presented in Figs. 2(d) and S1(a).

The NH_3 production rate was calculated as follows:

$$r_{NH3}\ (\text{mol h}^{-1}\ \text{cm}^{-2}) = (C_{NH3}\ \text{x}\ V) / (t\ \text{x}\ A), \quad (3)$$

where C_{NH3} is the molar concentration of NH_3 determined using the calibration curve obtained from UV–vis absorption spectra, V is the electrolyte volume, t is the reaction time, and A is the geometrical area of the electrode.

The FE was calculated by using.

$$\text{FE} = ((3F\ \text{x}\ V\ \text{x}\ C_{NH3})/\ Q)\ \text{x}\ 100, \quad (4)$$

where F is the Faraday constant (96,485 C mol^{-1}) and Q is the total charge passing through the electrochemical reaction.

The Watt and Chrisp method was employed to determine the potential byproduct of electrochemical NH_3 production, i.e., hydrazine (N_2H_4). An indicator solution consisting of 6 g of para(dimethylamino) benzaldehyde ($(CH_3)_2NC_6H_4CHO$), 30 mL of hydrochloric acid (HCl,

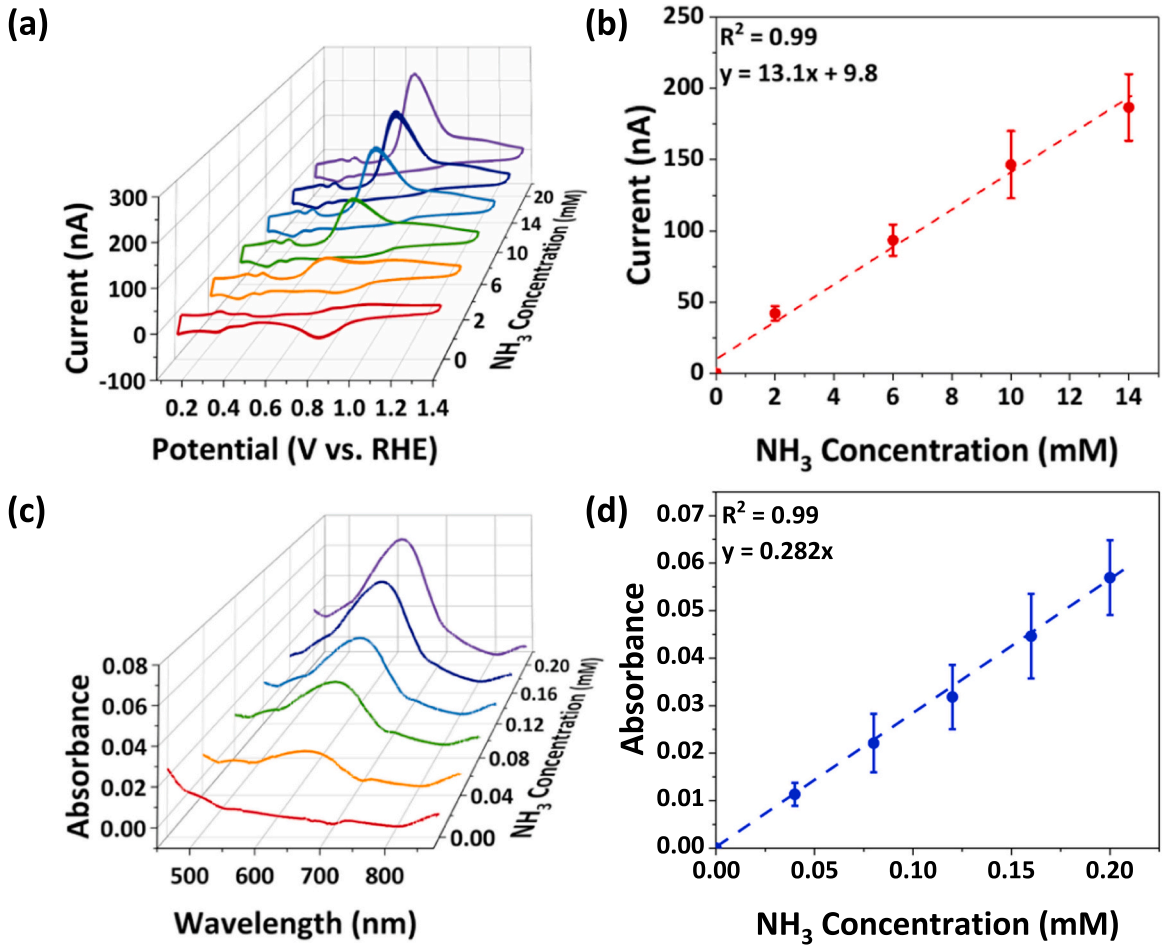

Fig. 2. (a) Cyclic voltammograms at the modified Pt UME in 1 M KOH aqueous solution including NH_3 at concentrations ranging from 0 to 20 mM with a scan rate of 20 mV s^{-1}. (b) The relationship between NH_3 concentration in 1 M KOH and AOR peak current in 1 M KOH aqueous solution. (c) UV–vis spectra of 1 M KOH including NH_3 at concentrations ranging from 0 to 0.2 mM. (d) The relationship between NH_3 concentration in 1 M KOH and UV–vis absorbance at a wavelength of 632 nm.

37%), and 300 mL of ethanol (C_2H_5OH) was used. After combining 2 mL of electrolyte with 2 mL of the indicator solution, the measurement was conducted. To quantify the amount of N_2H_4, a standard calibration curve was constructed using a series of dilutions of an $N_2H_4{\cdot}H_2O$ solution in 0.1 M KOH (Fig. S1(b)). The absorbance of N_2H_4 was evaluated at 456 nm using a UV–vis spectrometer.

2.7. Physical characterization

The crystalline structure of the e-NRR catalysts was characterized by X-ray powder diffraction (XRD) using a MiniFlex 2 X-ray diffractometer (Rigaku) with filtered Cu Kα radiation ($\lambda = 0.154$ nm) at 30 kV and 15 mA. The diffraction data were collected in the 2θ degree range of 10–90° with a scan rate of 2° min^{-1}. The electronic properties of the catalyst surface were characterized using X-ray photoelectron spectroscopy (XPS, Thermo Scientific K-Alpha) equipped with monochromated Al Kα radiation (1486.6 eV). All of the XPS spectra were corrected using adventitious C 1 s at 284.8 eV, and XPSPEAK 4.1 was used for XPS peak fitting.

3. Results and discussion

3.1. The AOR and NRR catalysts

To monitor the NH_3 produced via the e-NRR using SECM, polycrystalline Pt was layered on a UME with a diameter of 25 μm by using thermochemical deposition. Polycrystalline Pt was also deposited on a bulk Ti porous transport layer (PTL, 1 ×1 cm^2) to characterize the physical properties of the electrode. Via the XRD analysis, we identified the crystal structure of the Pt-coated Ti PTL as cubic Pt (PDF #65–2868; Fig. 1(b)). The size of the deposited Pt crystals was approximately 5 nm, as estimated by using the Scherrer equation and the full width at half maximum values of the (200) and (220) peaks at 46° and 68°. Given the size of the Pt UME (25 μm), the Pt nanoparticles on the UME provided a sufficiently large polycrystalline surface area for exposure to the electrolyte during the AOR. From the XPS analysis, the surface of the synthesized Pt was identified as including Pt^0, Pt^{2+}, and Pt^{4+} while the bulk of the Pt nanoparticles was metallic. The relative abundances of the Pt^0, Pt^{2+}, and Pt^{4+} were measured as 52%, 32%, and 16%, respectively (Fig. 1(c)). It is speculated that the surface of the metallic Pt nanoparticles was oxidized in the air after deposition on the UME.

For the e-NRR electrode, Fe-CuS/C was produced as reported in previous research [11]. As can be seen in the XRD pattern in Fig. 4(c), the prepared catalyst exhibited the CuS hexagonal phase (JCPDS #65–3566). The oxidation states of Cu were confirmed in the Cu 2p spectrum of the XPS analysis shown in Fig. 4(d): the percentages of Cu (II) and Cu(I) were 64% and 36%, respectively, indicating the presence of mixed CuS and copper(I) sulfide (Cu_2S) phases. The physical and chemical properties were the same as those reported in a previous study [11].

3.2. AOR activity

AOR electrodes were developed for use in the SECM probe designed to detect NH_3 dissolved in an aqueous solution. A commercially available Pt UME with a diameter of 25 μm was initially considered for use as the AOR electrode because Pt is a well-known active AOR catalyst [24]. A pristine unmodified Pt UME was immersed in 1 M KOH with different NH_3 concentrations (0, 10, and 20 mM; Fig. S2(a)). The untreated Pt UME displayed a broad oxidation current at 0.71 V_{RHE} in the presence of NH_3. The anodic peak currents at 0.71 V_{RHE} for 10 and 20 mM NH_3 was 4.3 and 6.1 nA, respectively. This measured AOR current was substantially lower than the theoretical mass transfer limiting current (538 nA) for a 25 μm UME, which is calculated as follows:

$$i_{mass\text{-}limit} = 4nFDC^*r_0 \quad (5)$$

where n is the number of electrons ($n = 6$), $F = 96{,}485$ C mol^{-1}, D is the diffusion coefficient for NH_3 in water (1.86 $\times 10^{-5}$ cm^2 s^{-1}), [25] C^* is the bulk concentration of NH_3 (10^{-5} mol cm^{-3}), and r^0 is the geometric radius of the UME (12.5 $\times 10^{-4}$ cm). The lower current observed for the AOR suggests that the AOR current is controlled by the kinetics of the reaction, with intermediate N-species on the surface preventing an increase in the AOR current at a more positive potential. In contrast, the pristine UME exhibited mass-limiting S-shaped CV curves when the reversible redox couple ferro/ferricyanide ($Fe(CN_6)^{2-/3-}$) was added to the solution (Fig. S3(a)).

As the unmodified Pt UME provided an AOR current that was only 0.8% of the mass-limiting current, a polycrystalline Pt UME with a larger surface area was fabricated by using thermochemical deposition. The surface area of the modified Pt UME was estimated in a 5 mM $Fe(CN_6)^{3-/4-}$ solution followed by CV measurements for AOR analysis in aqueous 1 M KOH solutions with 0, 2, 6, 10, 14, and 20 mM NH_3 (Fig. S4). The surface area of the modified Pt UME was 2.5 times higher and the reduction current for $Fe(CN_6)^{3-}$ increased from 21 to 53 nA compared with the unmodified Pt UME (Fig. S3(a)). The H-UPD (underpotential deposition) peaks for the Pt surface were also clearly enhanced following surface modification of the UME, thereby confirming that the surface area of the Pt UME had increased (Fig. S3(b)).

The AOR current increased considerably with the polycrystalline Pt nanoparticles on the modified Pt UME (Fig. S2(b)). For example, the AOR currents at 0.71 V_{RHE} for the unmodified and modified UMEs were 4.3 and 167.6 nA, respectively. This increase was larger than what could be expected solely from the larger surface area produced via tip modification, indicating that the enhancement of the AOR current occurred not only due to the increased surface area but also due to the facile AOR kinetics induced by the Pt nanoparticles on the Pt UME. [25] In particular, according to electrochemical analysis, 6.4% of the increase was from the higher surface area, and 93.6% was from the improved AOR kinetics. The reduction current for Pt oxide at 0.78 V_{RHE} also disappeared with the higher AOR current, as can be seen in Figs. S2(b) and 1(d). It is well known that the formation of a NO_x layer interferes with Pt oxide formation and reduction during the AOR [26]. However, the Pt oxidation and reduction peaks for the Pt UME were observed again when the solution was replaced with one without NH_3, indicating that the surface NO_x layer was easily removed. The cathodic current at around 0.5 V_{RHE} increased in the presence of NH_3, indicating the reduction of the AOR adsorbate [27]. In addition, the hydrogen adsorption/desorption peak shifted to a negative potential with NH_3 present in the electrolyte, indicating that the hydrogen binding energy on the Pt surface was reduced due to electrostatic interaction with NH_3 [24].

The relationship between NH_3 concentration and AOR current for the Pt UME was also investigated. As shown in Fig. 2(b), a first-order relationship with high precision was derived for the Pt UME (the measurements were taken at least three times at each NH_3 concentration). To produce the standard calibration curve, the charging current observed at 0.47 V_{RHE} was used as the background current and subtracted from the peak AOR current shown in Fig. 2(a). The standard curve for the experimental relationship between NH_3 concentration and AOR current was then used to estimate the NH_3 concentration produced by the e-NRR electrode. In addition to the electrochemical analysis, UV–vis spectroscopy and colorimetry were conducted to measure the NH_3 concentration in the solution (Fig. 2(c)). A linear relationship between NH_3 concentration and AOR peak current in the CV analysis was clearly observed for NH_3 concentrations up to 20 mM (Fig. S5(a)). However, at higher concentrations (Fig. S5(b)), the reaction was influenced by factors other than the concentration, such as surface interference and local pH changes, thus the AOR current was no longer directly proportional to the NH_3 concentration [24,28]. The AOR current gradually became saturated at higher NH_3 concentrations, which limited the electrochemical NH_3 detection to 14 mM in this study.

3.3. NH_3 detection in TC-mode SECM

The use of the AOR at the Pt UME for NH_3 detection via SECM was first examined using a homemade model substrate designed to release NH_3 at a controlled concentration of 10 mM in an aqueous 1 M KOH solution via a mechanically fabricated disk hole with a diameter of 250 μm (Fig. 3(a)). The substrate was made of polyether ether ketone, and the Pt UME tip was positioned by a normal negative feedback mode of SECM before NH_3 detection. The Pt UME was positioned over the hole at a distance of 30 μm between the UME and substrate, and the NH_3 release hole was covered with Kapton film. During this process, the position of the substrate relative to the UME was controlled using three-point level adjustment. The location of the protective film was then visualized via the mapping of the Pt UME over an area of 1.8 × 1.2 mm^2 around the protective film. In the surface scan, the negative feedback current at the Pt UME at 0.41 V_{RHE} was recorded in 5 mM $K_3Fe(CN)_6$/$K_4Fe(CN)_6$ and an aqueous 1 M KCl solution (Fig. S6). Once the area for investigation was identified, area mapping was conducted again in an aqueous 1 M KOH solution with a smaller mapping area of 600 × 800 μm^2 after peeling off the protective film. In the second mapping step, the potential of the UME was fixed at 0.71 V_{RHE} (the potential used for actual AOR measurements) to observe the background current at the Pt UME in the absence of NH_3 in the solution.

The NH_3 that diffused into the 1 M KOH solution from the release hole of the model substrate was then monitored (Fig. 3(b)). Under the SECM mapping mode, the Pt UME tip was held at 0.71 V_{RHE} while the tip current was recorded via CA. During the area mapping process, a higher concentration of NH_3 represented by a higher AOR current was observed around the release hole of 10 mM NH_3. An AOR current of up to 0.21 nA at the Pt UME was measured via CA measurement of the area mapping, whereas a reduction current was observed for the NH_3-free solution (Fig. 3(c)). However, the AOR current during area mapping was notably lower than that observed with the Pt UME under CV mode; the Pt UME measurements at the center of the release hole provided an AOR peak current of 61.1 nA at d = 30 μm (Fig. 3(d)), which was approximately 291 times higher than that during area mapping. It has been reported that the transient AOR current rapidly decreases at a fixed potential due to reaction intermediates from the AOR being adsorbed on the active catalytic sites [29]. The AOR current from the CV measurements was also affected by the distance between the Pt UME and the release hole in the substrate (d). For example, the oxidation current at 0.71 V_{RHE} decreased to 1.7 nA at d = 1000 μm, which was considered as the background current without the AOR because the tip was located far from the substrate (i.e., a distance 10 times larger than the UME radius); the NH_3 released from the substrate was not considered to be detectable at that distance (Fig. 3(d)).

The AOR current at the Pt UME at d = 30 μm was approximately 42% compared to that at the Pt UME in a homogeneous 10 mM NH_3 in 1 M KOH solution (146.5 nA at 0.71 V_{RHE}; Fig. 2(b)). This implies that the local NH_3 concentration at d = 30 μm above the release hole would be 3.9 mM because the solution had been diluted with 1 M KOH and the collection efficiency of TC-SECM is 42% at d = 30 μm. The collection efficiency for NH_3 was approximately 2% lower than that for 10 mM $K_3Fe(CN)_6$/$K_4Fe(CN)_6$ at the same position. When the 10 mM NH_3 was replaced with 10 mM $K_3Fe(CN)_6$/$K_4Fe(CN)_6$ in the release hole experiment, a collection efficiency of 44% was observed with an identical Pt UME at d = 30 μm (Fig. S7(b)). The different collection efficiencies for NH_3 and Fe^{2+} oxidation could be the result of the different

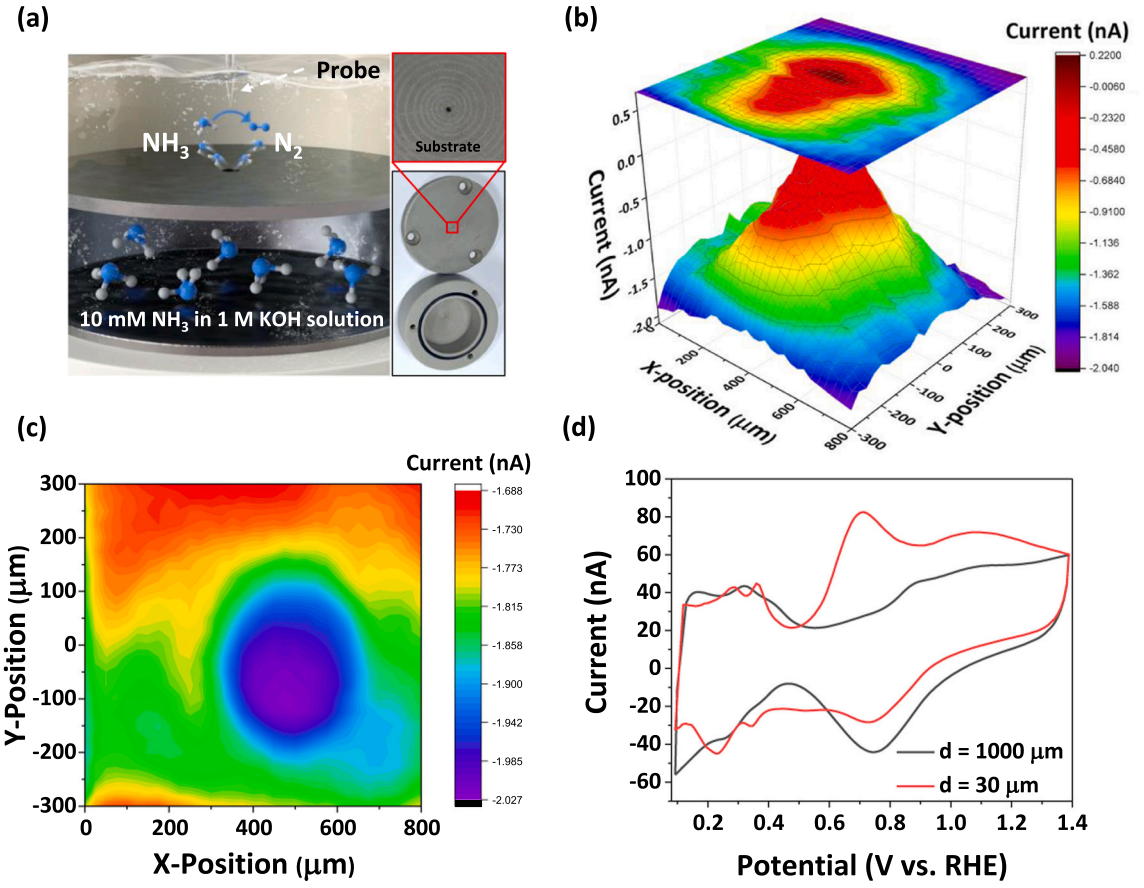

Fig. 3. (a) A schematic of NH_3 detection in TC-mode on SECM. (b) SECM area mapping of the model stage while the Pt UME was located in pure 1 M KOH aqueous solution and NH_3 was released from the bottom hole. (c) SECM area mapping image in the absence of NH_3 in 1 M KOH solution. (d) Cyclic voltammograms at the Pt UME in 1 M KOH solution with a distance of 30 μm and 1000 μm between the substrate hole and probe with a scan rate of 20 mV s^{-1}.

diffusion coefficients of the cations (1.86×10^{-5} and 7.2×10^{-6} cm^2 s^{-1} for NH_3 and Fe^{2+}, respectively) or other kinetic or interference effects on the reaction at the Pt UME [25,30,31]. As discussed above, the nitrogen adsorbate generated during the AOR has a high binding affinity with the Pt surface (394 kJ mol^{-1} for Pt(111)-N) and thus interferes with the AOR and decreases the oxidation current [29]. However, based on a comparison of the collection efficiencies using the NH_3 solution and $K_3Fe(CN)_6/K_4Fe(CN)_6$ via the model substrate, it was concluded that more than 95% of the NH_3 released by the substrate was detected by the CV-based analytical method at the Pt UME tip. This analytical result is similar to that for transient surface-interrogation of SECM (SI-SECM), and strongly binding adsorbates can be removed in consecutive scans. The collection efficiency can also be increased if the distance between the tip and the substrate is reduced, thereby increasing the resolution for NH_3 detection in SECM (see Fig. S7(c) and (d) showing model experiments using $K_3Fe(CN)_6/K_4Fe(CN)_6$ with lower *d* values).

3.4. e-NRR bulk activity of the Fe-CuS/C catalyst

Before SG-TC mode of SECM was used, the activity and durability of the Fe-CuS/C catalyst used as a bulk electrode were investigated via previously reported methodology [11]. A porous gas-diffusion electrode layered with Fe-CuS/C (2.5×2.5 cm^2) was prepared and placed in a nitrogen-purged 0.1 M KOH solution. The e-NRR reaction was carried out for 30 min over an applied potential range from 0.0 to −0.6 V_{RHE}. The amount of produced and accumulated NH_3 in the electrolyte was investigated using both the indophenol method and electrochemical analysis after the CA measurements. The NH_3 production rate (or NH_3

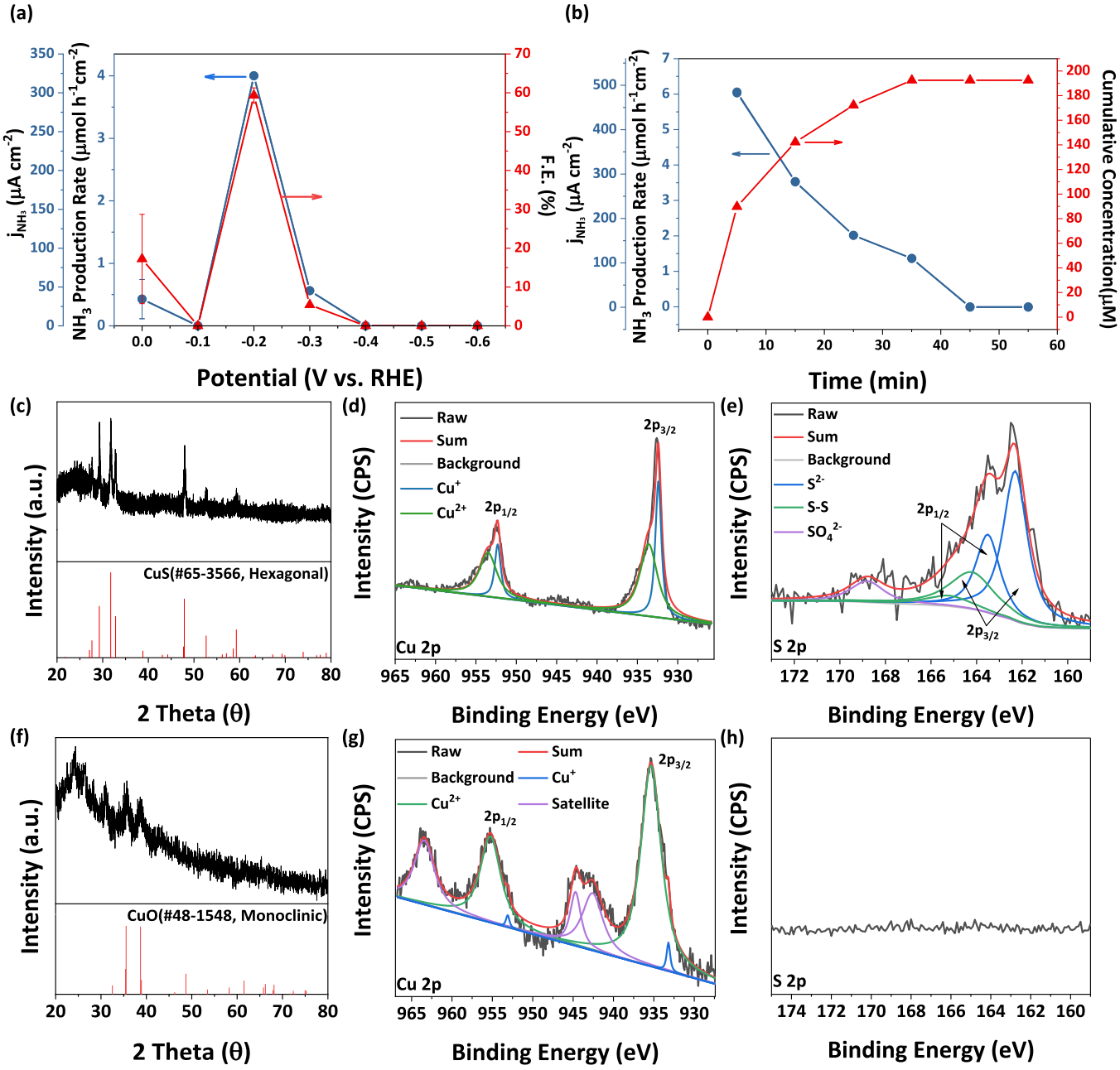

Fig. 4. (a) Current density, NH_3 production rate, and FE for electrochemical NH_3 synthesis of the 0.5 at% Fe-CuS/C catalyst at various applied potentials from 0 to − 0.6 V_{RHE}. (b) Durability test of the 0.5 at% Fe-CuS/C catalyst at −0.2 V_{RHE}. The NH_3 production rate and concentration were estimated via the indophenol method. (c) An XRD pattern and XPS (d) Cu 2p and (e) S 2p spectra of Fe-CuS/C before durability test. (f) An XRD pattern and XPS (g) Cu 2p and (h) S 2p spectra of Fe-CuS/C after durability test.

production partial current density) and the FE for each potential evaluated using colorimetry are shown in Fig. 4(a). A high NH_3 production rate of 4 μmol h^{-1} cm^{-2} and FE of 60% were observed at −0.2 V_{RHE}, with the reaction rate and FE decreasing with larger overpotentials. It has been reported that the lower activity and selectivity for the e-NRR at larger overpotentials is due to the facile HER at negative potentials and the limited stability of Fe-CuS/C catalysts [11,32]. The Watt and Chrisp method was used in an attempt to detect N_2H_4, a potential byproduct of the nitrogen-reduction reaction. However, N_2H_4 was not detected.

The durability of the Fe-CuS/C catalyst was also studied at −0.2 V_{RHE} and the concentration of NH_3 accumulated in the electrolyte solution was measured every 10 min for 1 h (Fig. 4(b)). At the beginning of the durability test, the highest NH_3 production rate (6 μmol cm^{-2} h^{-1}) and NH_3 production partial current (0.5 mA cm^{-2}) were observed. However, the NH_3 production rate decreased over time, and the NH_3 concentration in the electrolyte did not increase further after 50 min. The limited lifetime of the e-NRR catalyst was ascribed to the structural degradation of Fe-CuS/C to copper(II) oxide (CuO) during the e-NRR process [11]. This was verified via XRD and XPS analyses, which revealed the transition of Fe-CuS/C to CuO, thereby disrupting e-NRR catalysis (Fig. 4 (c–h)). The poor durability of sulfide catalysts has been widely reported, and Kim et al. [33] suggested a regeneration method for them that allows continuous e-NRR operation.

3.5. SG-TC mode of SECM

The activity and durability of the Fe-CuS/C catalyst were investigated under SG-TC mode of SECM (Fig. 5(a)). Based on the results of the analysis of the bulk e-NRR electrode, the potential applied to the Fe-CuS/C-coated gas-diffusion electrode was −0.2 V_{RHE} (Fig. S8). The Pt UME tip was located 100 μm above the Fe-CuS/C catalyst, and CV analysis at the Pt UME was conducted to observe the AOR current. The solution was nitrogen-purged 1 M KOH and the AOR current at the Pt UME was calibrated in the solution before SG-TC mode of SECM was conducted. When comparing 0.1 M and 1 M KOH solutions, the AOR current was higher in the more concentrated one (Fig. S9) [34]. It is known that the AOR has a lower onset potential and a higher AOR current at higher OH^- concentrations due to facile charge transfer kinetics. [33] Before the actual interrogation, an approach curve of the Pt UME was constructed with an insulating polymer film covering the e-NRR electrode (Fig. S10). The tip–substrate distance was estimated by simulating the approach curve at RG = 10 (Table S1). SG-TC mode of SECM was carried out on the Fe-CuS/C electrode and Pt UME, after which the following reactions proceeded:

Substrate Generation (SG, e-NRR): $N_2 + 6\,H_2O + 6e^- \rightarrow 2NH_3 + 6OH^-$ (6)

Tip Collection (TC, AOR): $2NH_3 + 6OH^- \rightarrow N_2 + 6\,H_2O + 6e^-$ (7)

In SG-TC mode of SECM, a clear AOR current was detected from the

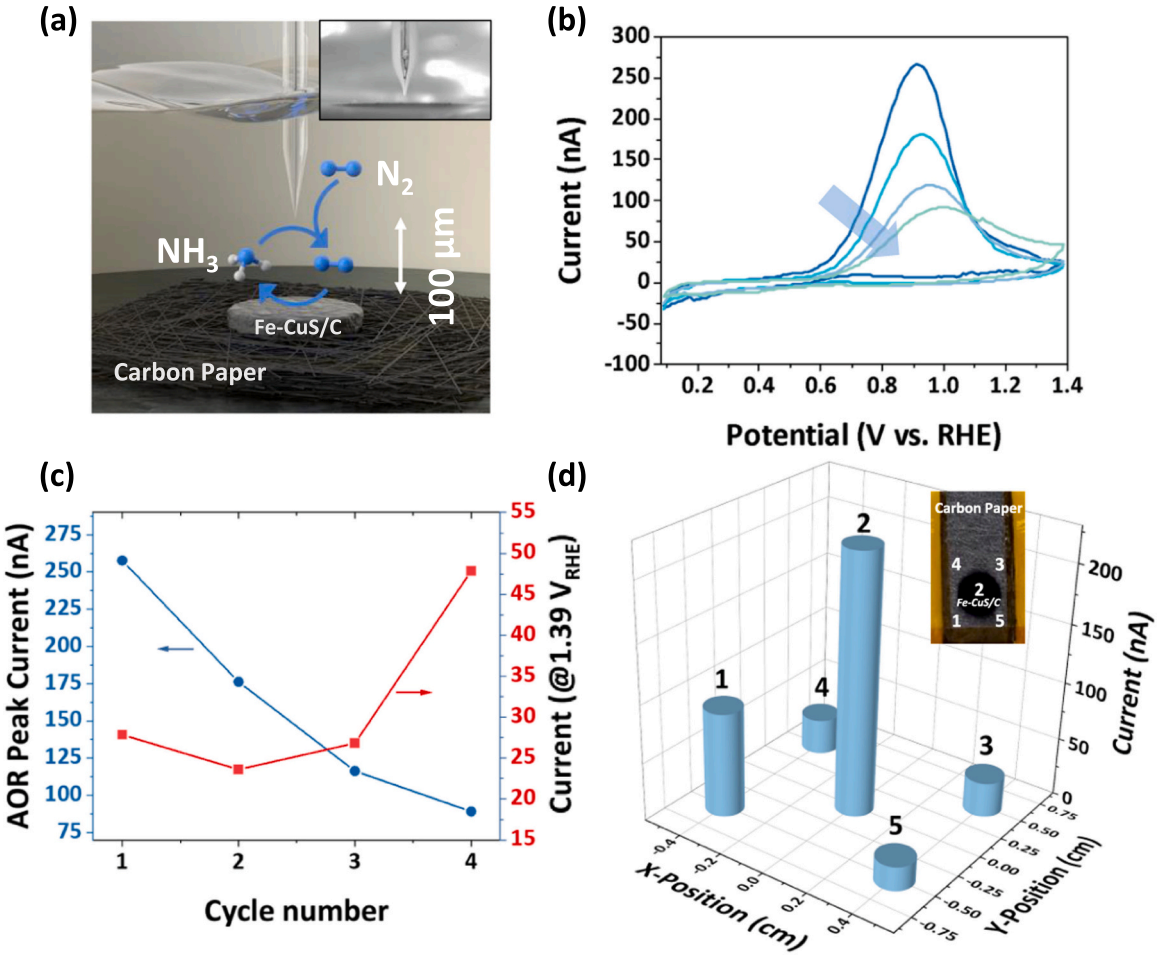

Fig. 5. (a) A schematic diagram of the SECM SG-TC mode using catalyst-loaded carbon paper for the e-NRR and the Pt UME for the AOR. The inset is an actual image of the experimental setup. (b) Cyclic voltammograms at the Pt UME in the potential ranged from 0.09 to 1.39 V_{RHE} at a scan rate of 20 mV s^{-1}. (c) The AOR peak current at around 0.9 V_{RHE} and the S^{2-} oxidation current at 1.39 V_{RHE} in repeated CV scans. (d) Point-mapping results over the substrate at five different positions (inset: the e-NRR catalyst layered on carbon paper with the measured position indicated). The AOR current was obtained at 0.97 V_{RHE} in the cyclic voltammograms (Fig. S14).

Pt UME positioned near the Fe-CuS/C electrode, meaning that the NH_3 produced electrochemically at the e-NRR electrode was observed *in-situ* (Fig. 5(b)). The peak AOR current from the Pt UME was 258 nA at 0.91 V_{RHE}, which corresponds to a local NH_3 concentration of 18.9 mM in the electrolyte. Given the collection efficiency at $d = 100$ μm of 28%, the local NH_3 concentration at the surface of the e-NRR electrode was estimated to be 67.2 mM. Considering the average roughness (Ra) of the e-NRR electrode measured as 8.76 μm on the optical profilometer, approximately a 3% of detection error could occur at $d = 100$ μm. Besides, the AOR current also continuously decreased in sequential CV scans, thereby confirming the limited durability of the e-NRR electrode.

The Pt UME could also be used to observe a number of interesting analytical features related to the degradation of the Fe-CuS/C electrode during the e-NRR process. For example, the cyclic voltammogram at the Pt UME above the Fe-CuS/C electrode did not contain H-UPD and H desorption peaks and the onset potential for the AOR shifted to a more positive potential with repeated CV scans while the AOR peak current decreased. In addition, the new oxidation current at 1.39 V_{RHE} increased with a higher number of CV scans (Fig. 5(c)). These observations suggest that the AOR at the Pt UME was hindered when the e-NRR activity of Fe-CuS/C was degraded. However, the disappearance of H-UPD and the increase in oxidation current at 1.39 V_{RHE} were not directly related to the decreased NH_3 production rate at the e-NRR. As shown in Fig. 1(d), H-UPD and H desorption peaks should be observable in the presence of the AOR, which is not the case in the CV scans at the Pt UME shown in Fig. 5(b). Similarly, the higher AOR overpotential and new oxidation current at 1.39 V_{RHE} were not directly related to the decreased NH_3 concentration at the Pt UME. Rather, it is speculated that the transient phenomena observed at the Pt UME in SG-TC mode of SECM originated from the degradation mechanisms of the e-NRR catalyst investigated in the present study. In particular, it has been reported that Fe-CuS/C degrades to CuO when used as an e-NRR catalyst during the NH_3 production process [11]. In the decomposition of Fe-CuS to CuO, sulfide ions (S^{2-}) are generated and diffuse into the solution, which can be strongly adsorbed to the Pt UME and interfere with the active sites for the AOR and H-UPD [35,36].

To prove the effect of sulfide ions on the TC signal of SECM, CV analysis at the Pt UME was conducted for concentrations of sodium sulfide (Na_2S) up to 5 mM in an aqueous 1 M KOH solution (Fig. S11). As the concentration of Na_2S was increased, the peaks for $H_{adsorption}/H_{desorption}$ at the Pt UME gradually decreased. In addition, a reduction in AOR activity at Pt UME was clearly observed with the concentration of Na_2S as low as 0.02 mM in 20 mM NH_3 and 1 M KOH. At Na_2S concentrations of less than 0.8 mM, an increase in the oxidation current at 1.39 V_{RHE}, which corresponds to sulfide oxidation at the Pt UME, was not clearly observed for the AOR. However, a sulfide oxidation current was clearly observed at Na_2S concentrations higher than 0.8 mM (Fig. S11(b)). The oxidation current was approximately 60 nA for 0.8 mM Na_2S, which is similar to that observed at the Fe-CuS/C electrode in Fig. 5(b). This implies that the detection of NH_3 with a concentration of 18.9 mM in solution was effectively inhibited by the presence of S^{2-} at a concentration of less than 4% of the NH_3 (0.8 mM) in SG-TC mode of SECM using the Pt UME. This also suggests that the NH_3 concentration measured by using the Pt UME may be underestimated by the S^{2-} interference effect. However, the H-UPD, H oxidation, and AOR currents at the Pt UME, which were difficult to observe due to surface interference by the sulfide ions, were recovered after repeated CV scans in clean 1 M KOH (Fig. S12).

Overall, the transient behavior of the tip current for the Pt UME was the result of two factors: (a) a decrease in the NH_3 production rate at the Fe-CuS/C electrode due to catalyst degradation and (b) the inhibitory effect of S^{2-} released from the Fe-CuS/C during the AOR at the Pt UME. Under SG-TC mode of SECM, the NH_3 generated on the e-NRR substrate was clearly detectable in real-time via the oxidation reaction of the Pt UME, which also enabled monitoring of the degradation behavior. It is also possible that the estimated NH_3 concentration under SG-TC mode of SECM was underestimated in part because the probe activity was hindered by the sulfide ions generated during the e-NRR process.

As a background experiment for the use of SG-TC mode of SECM for NH_3 detection, pristine carbon paper without the e-NRR catalyst was examined at the same potential of −0.2 V_{RHE} in a nitrogen-purged 1 M KOH solution ($d = 100$ μm; Fig. S13). In the experiment, an AOR current was not observed at the Pt UME, indicating that the AOR signal detected above the Fe-CuS/C electrode was the result of the catalytic activity of the e-NRR substrate. In addition, no changes at the Pt UME, such as that due to the S^{2-} interference effect, were observed.

Finally, point mapping under SG-TC of SECM was conducted over the Fe-CuS/C catalyst to demonstrate local NH_3 production. Ideally, SECM analysis should provide a continuous activity map over the target electrode by modulating the XYZ position of the UME [37]. However, area mapping of the SECM was not conducted because the e-NRR catalyst had limited durability, which did not allow for long-term measurements. Therefore, schematic point-of-activity mapping for the Fe-CuS/C electrode was conducted at five different points with a scan rate of 100 mV s^{-1} (Fig. S14(a)). Fig. 5(d) shows the average oxidation current at 0.97 V_{RHE} measured in cyclic voltammograms at five different positions. From the results, the AOR only occurred above the e-NRR catalyst, and the AOR peak was not observed in the cyclic voltammograms when the tip was moved far away from the e-NRR catalyst (Fig. S14(b–f)). Although the acquired space coordinate information for e-NRR activity was limited due to the low stability of the e-NRR electrode, the operating principles for SECM in the *in-situ* detection of NH_3 were clearly demonstrated under SG-TC mode of SECM over the Fe-CuS/C catalyst.

In this study, the *in-situ* detection of electrochemically generated NH_3 using SECM was demonstrated for the first time. A low NH_3 flux of 6.6 nmol cm^{-2} s^{-1} produced at the Fe-CuS/C electrode (Fig. S15) was observed from the AOR on a polycrystalline Pt UME with a diameter of 25 μm. The real-time observations provide invaluable information on the e-NRR, including transient activity and durability. The advantages and limitations of the proposed *in-situ* NH_3 detection method using SECM are clearly demonstrated in the evaluation of the e-NRR, and this approach has the potential to facilitate the development of e-NRR catalysis.

4. Conclusions

In the present study, *in-situ* analytical SECM was used for the first time to evaluate e-NRR catalysis. Under SG-TC mode of SECM, the NH_3 electrochemically produced at an Fe-CuS/C electrode via the e-NRR could be detected and provided pertinent information on the transient activity and durability of the catalytic system with space coordinate values. To apply SECM to e-NRR research, a polycrystalline Pt UME was fabricated with enhanced AOR activity, while the quantitative relationship between the local NH_3 concentration and the collection efficiency of the fabricated Pt UME was demonstrated, with an NH_3 collection efficiency of 42% observed when the tip was 30 μm above the NH_3 production site. The local NH_3 concentration detected in the vicinity of the e-NRR electrode using SECM was up to 145 times higher than that measured in the bulk solution using *ex-situ* techniques. The results indicate that smaller e-NRR electrodes with a high local NH_3 concentration can be evaluated using SECM, whereas other *ex-situ* techniques require a much higher bulk concentration of NH_3 using larger electrodes or else a longer experimental duration. In addition, the real-time detection of NH_3 using SECM allows for the evaluation of e-NRR catalysts with limited stability, as demonstrated by the Fe-CuS/C catalyst in the present study. The real-time activity of a catalyst for electrochemical NH_3 synthesis and information on the transient degradation process for the catalyst can be obtained using SECM analysis of e-NRR electrodes. We believe the detection of NH_3 using the proposed SECM method opens a new route for the development of effective e-NRR catalysts by providing invaluable information on nitrogen-reduction catalysis that cannot be obtained via currently available analytical

techniques.

CRediT authorship contribution statement

Jimin Kong: Experiment, Data analysis, Writing – original draft, Writing – review & editing. **Hansung Kim**: Visualization, Data curation, Writing – review & editing, Supervision. **Hyun S. Park**: Conceptualization, Funding acquisition, Investigation, Writing – original draft, Writing – review & editing, Supervision.

Declaration of Competing Interest

The authors declare that they have no known competing financial interests or personal relationships that could have appeared to influence the work reported in this paper.

Acknowledgements

This work was supported by the Creative Materials Discovery Program through the National Research Foundation of Korea (NRF-2021M3D1A2051389) and the Korea Institute of Science and Technology (2E32591).

Appendix A. Supporting information

Supplementary data associated with this article can be found in the online version at doi:10.1016/j.apcatb.2023.123019.

References

[1.] S. Ghavam, M. Vahdati, I.A.G. Wilson, P. Styring, Sustainable ammonia production processes, Front. Energy Res. (2021) *9*.
[2.] M. Neghab, A. Mirzaei, H. Jalilian, M. Jahangiri, J. Zahedi, S. Yousefinejad, Effects of low-level occupational exposure to ammonia on hematological parameters and kidney function, Int J. Occup. Environ. Med 10 (2) (2019) 80–88.
[3.] H. Wang, Y. Chen, R. Fan, J. Chen, Z. Wang, S. Mao, Y. Wang, Selective electrochemical reduction of nitrogen to ammonia by adjusting the three-phase interface, Research 2019 (2019) 1401209.
[4.] V. Smil, Detonator of the population explosion, Nature 400 (6743) (1999), 415-415.
[5.] J. Cha, T. Lee, Y.-J. Lee, H. Jeong, Y.S. Jo, Y. Kim, S.W. Nam, J. Han, K.B. Lee, C. W. Yoon, H. Sohn, Highly monodisperse sub-nanometer and nanometer Ru particles confined in alkali-exchanged zeolite Y for ammonia decomposition, Appl. Catal. B: Environ. 283 (2021), 119627.
[6.] H.S. Kim, H. Jin, S.-H. Kim, J. Choi, D.W. Lee, H.C. Ham, S.J. Yoo, H.S. Park, Sacrificial Dopant to Enhance the Activity and Durability of Electrochemical N2 Reduction Catalysis, ACS Catal. 12 (9) (2022) 5684–5697.
[7.] J. Wang, S. Chen, Z. Li, G. Li, X. Liu, Recent advances in electrochemical synthesis of ammonia through nitrogen reduction under ambient conditions, ChemElectroChem 7 (5) (2020) 1067–1079.
[8.] J. Kong, A. Lim, C. Yoon, J.H. Jang, H.C. Ham, J. Han, S. Nam, D. Kim, Y.-E. Sung, J. Choi, Electrochemical synthesis of NH3 at low temperature and atmospheric pressure using a γ-Fe2O3 catalyst, ACS Sustain. Chem. Eng. 5 (11) (2017) 10986–10995.
[9.] W. Yu, N.S. Lewis, H.B. Gray, N.F. Dalleska, Isotopically selective quantification by UPLC-MS of aqueous ammonia at submicromolar concentrations using dansyl chloride derivatization, ACS Energy Lett. 5 (5) (2020) 1532–1536.
[10.] Y. Zhao, R. Shi, X. Bian, C. Zhou, Y. Zhao, S. Zhang, F. Wu, G.I.N. Waterhouse, L.-Z. Wu, C.-H. Tung, T. Zhang, Ammonia detection methods in photocatalytic and electrocatalytic experiments: how to improve the reliability of NH3 production rates? Adv. Sci. 6 (8) (2019) 1802109.
[11.] J. Kong, M.-S. Kim, R. Akbar, H.Y. Park, J.H. Jang, H. Kim, K. Hur, H.S. Park, Electrochemical nitrogen reduction kinetics on a copper sulfide catalyst for NH3 synthesis at low temperature and atmospheric pressure, ACS Appl. Mater. Interfaces 13 (21) (2021) 24593–24603.
[12.] G. Qing, R. Ghazfar, S.T. Jackowski, F. Habibzadeh, M.M. Ashtiani, C.-P. Chen, M. R. Smith, I.I.I. Hamann, T. W., Recent Advances and Challenges of Electrocatalytic N2 Reduction to Ammonia, Chem. Rev. 120 (12) (2020) 5437–5516.
[13.] K. Krempl, D. Hochfilzer, F. Cavalca, M. Saccoccio, J. Kibsgaard, P.C.K. Vesborg, I. Chorkendorff, Quantitative operando detection of electro synthesized ammonia using mass spectrometry, ChemElectroChem 9 (6) (2022), e202101713.
[14] D. Ripepi, R. Zaffaroni, M. Kolen, J. Middelkoop, F.M. Mulder, Operando isotope selective ammonia quantification in nitrogen reduction studies via gas chromatography-mass spectrometry, Sustain. Energy Fuels 6 (8) (2022) 1945–1949.
[15] A.J. Bard, F.R.F. Fan, J. Kwak, O. Lev, Scanning electrochemical microscopy, Introd. Princ. *Anal. Chem.* 61 (2) (1989) 132–138.
[16] S.V. Kalinin, A. Gruverman, Scanning Probe Microscopy: Electrical and Electromechanical Phenomena at the Nanoscale, Springer Science & Business Media,, 2007.
[17] F.D. Mayer, P. Hosseini-Benhangi, C.M. Sánchez-Sánchez, E. Asselin, E.L. Gyenge, Scanning electrochemical microscopy screening of CO_2 electroreduction activities and product selectivities of catalyst arrays, Commun. Chem. 3 (1) (2020) 155.
[18] X. Wang, G. Askarova, M.V. Mirkin, Chapter 4 - Electrochemical microscopy at the nanoscale, in: A.J. Wain, E.J.F. Dickinson (Eds.), In *Frontiers of Nanoscience*, Vol. 18, Elsevier, 2021, pp. 129–202.
[19] G. Lu, J.S. Cooper, P.J. McGinn, SECM imaging of electrocatalytic activity for oxygen reduction reaction on thin film materials, Electrochim. Acta 52 (16) (2007) 5172–5181.
[20] H.S. Ahn, A.J. Bard, Surface Interrogation Scanning Electrochemical Microscopy of Ni1–xFexOOH (0 < x < 0.27) Oxygen Evolving Catalyst: Kinetics of the "fast" Iron Sites, J. Am. Chem. Soc. 138 (1) (2016) 313–318.
[21] D. Gupta, S. Chakraborty, R.G. Amorim, R. Ahuja, T.C. Nagaiah, Local electrocatalytic activity of PtRu supported on nitrogen-doped carbon nanotubes towards methanol oxidation by scanning electrochemical microscopy, J. Mater. Chem. A 9 (37) (2021) 21291–21301.
[22] P. Sun, F.O. Laforge, M.V. Mirkin, Scanning electrochemical microscopy in the 21st century, Phys. Chem. Chem. Phys. 9 (7) (2007) 802–823.
[23] L. Zhou, C.E. Boyd, Comparison of Nessler, phenate, salicylate and ion selective electrode procedures for determination of total ammonia nitrogen in aquaculture, Aquaculture 450 (2016) 187–193.
[24] Z.-F. Li, Y. Wang, G.G. Botte, Revisiting the electrochemical oxidation of ammonia on carbon-supported metal nanoparticle catalysts, Electrochim. Acta 228 (2017) 351–360.
[25] J.U. Kreft, C. Picioreanu, J.W. Wimpenny, M.C. van Loosdrecht, Individual-based modelling of biofilms, Microbiol. (Read., Engl.) 147 (Pt 11) (2001) 2897–2912.
[26] S. Johnston, B.H.R. Suryanto, D.R. MacFarlane, Electro-oxidation of ammonia on electrochemically roughened platinum electrodes, Electrochim. Acta 297 (2019) 778–783.
[27] H. Kim, M.W. Chung, C.H. Choi, NOx-induced deactivation of Pt electrocatalysis towards the ammonia oxidation reaction, Electrochem. Commun. 94 (2018) 31–35.
[28] C. Zhong, W.B. Hu, Y.F. Cheng, Recent advances in electrocatalysts for electro-oxidation of ammonia, J. Mater. Chem. A 1 (10) (2013) 3216–3238.
[29] H. Kim, W. Yang, W.H. Lee, M.H. Han, J. Moon, C. Jeon, D. Kim, S.G. Ji, K.H. Chae, K.-S. Lee, J. Seo, H.-S. Oh, H. Kim, C.H. Choi, Operando Stability of Platinum Electrocatalysts in Ammonia Oxidation Reactions, ACS Catal. 10 (19) (2020) 11674–11684.
[30] J. Moldenhauer, M. Meier, D.W. Paul, Rapid and direct determination of diffusion coefficients using microelectrode arrays, J. Electrochem. Soc. 163 (8) (2016) H672.
[31] H.S. Park, J.H. Jang, Applications of Scanning Electrochemical Microscopy (SECM) Coupled to Atomic Force Microscopy with Sub-Micrometer Spatial Resolution to the Development and Discovery of Electrocatalysts, J. Electrochem. Sci. Technol. 7 (4) (2016) 316–326.
[32] D. Bao, Q. Zhang, F.L. Meng, H.X. Zhong, M.M. Shi, Y. Zhang, J.M. Yan, Q. Jiang, X.B. Zhang, Electrochemical reduction of N2 under ambient conditions for artificial N2 fixation and renewable energy storage using N2/NH3 cycle, Adv. Mater. 29 (3) (2017) 1604799.
[33] H.S. Kim, J. Choi, J. Kong, H. Kim, S.J. Yoo, H.S. Park, Regenerative electrocatalytic redox cycle of copper sulfide for sustainable NH3 production under ambient conditions, ACS Catal. 11 (1) (2020) 435–445.
[34] Y. Zhao, B.P. Setzler, J. Wang, J. Nash, T. Wang, B. Xu, Y. Yan, An efficient direct ammonia fuel cell for affordable carbon-neutral transportation, Joule 3 (10) (2019) 2472–2484.
[35] C.-H. Chen, C. Brennan, S.C.S. Lai, D.J. Fermin, P.R. Unwin, P. Rodriguez, Adsorption and Electrochemical Oxidation of Small Sulfur−Containing Anions on Pt Electrodes in Organic Media, ChemElectroChem 5 (16) (2018) 2228–2234.
[36] C.-H. Chen, A. Halford, M. Walker, C. Brennan, S.C.S. Lai, D.J. Fermin, P.R. Unwin, P. Rodriguez, Electrochemical characterization and regeneration of sulfur poisoned Pt catalysts in aqueous media, J. Electroanal. Chem. 816 (2018) 138–148.
[37] H.S. Park, K.E. Kweon, H. Ye, E. Paek, G.S. Hwang, A.J. Bard, Factors in the Metal Doping of BiVO4 for Improved Photoelectrocatalytic Activity as Studied by Scanning Electrochemical Microscopy and First-Principles Density-Functional Calculation, J. Phys. Chem. C. 115 (36) (2011) 17870–17879.